Indian Journal of Chemistry
Vol. 60A, January 2021, pp. 51-61

Computational structure characterization, nonlinear optical properties and antitumor activities of Nickel(II) complexes containing alkoxy-derived dicyandiamide ligands

Tuba Alagöz Sayın & Duran Karakaş*

Sivas Cumhuriyet University, Science Faculty, Chemistry Department, 58140 Sivas, Turkey

*E-mail: dkarakas@cumhuriyet.edu.tr

Received 18 June 2020; revised and accepted 05 October 2020

$[Ni(dcda\text{-}O\text{-}Me)_2]^{2+}$ **(1)**, $[Ni(dcda\text{-}O\text{-}Et)_2]^{2+}$ **(2)**, $[Ni(dcda\text{-}O\text{-}nPr)_2]^{2+}$ **(3)**, and $[Ni(dcda\text{-}O\text{-}nBu)_2]^{2+}$ **(4)** complexes (dcda-O-R is dicyandiamide ligands with alkoxy-derived) have been optimized in the gas phase at B3LYP/LANL2DZ/6-31+G(d,p) level. Computational structure characterization has been performed from the structural parameters, IR spectra, ^{1}H-NMR, ^{13}C-NMR chemical shift values. It has been found that the central metal atom geometry in the complexes is a distorted square plane. Some electronic structure descriptors of the complexes are calculated in the gas phase and nonlinear optical properties are predicted. Complex **1** is found as the most suitable compound to produce optical material. The complexes are optimized at the same level in the aqueous phase to determine antitumor activity. Some electronic structure descriptors are calculated and molecular docking calculations are made against the 3WZE protein. According to the calculated electronic structure descriptors and molecular docking results, it is found that the complex **3** has the highest antitumor activity against the selected target protein.

Keywords: Dicyandiamide, Ni(II) complexes, Computational structure characterization, NLO properties, Antitumor activity

Dicyandiamide (dcda) is a ligand having two tautomeric structures as N≡C–N=C$(NH_2)_2$ and N≡C-NHC(=NH)NH_2. As seen from tautomeric structures, the dcda ligand contains a nitrile group (N≡C-). Nitrile is an active group and forms dicyandiamide derivatives by giving nucleophilic addition reactions with water, alcohols, and amines in the presence of transition metal ions. While guanylurea is formed by the nucleophilic addition of water to dicyandiamide, 1-amidino-O-alkylurea is formed by the nucleophilic addition of alcohols, and biguanides are formed from the nucleophilic addition of amines[1-5]. There is no significant reaction between dicyandiamide and alcohols when there is no metal ion. However, the addition of alcohol to dicyandiamine in the presence of the Cu(II) ion results in high yields, while the same reaction takes a long time in the presence of Ni(II), requires a base, and the yield is low[6,7].

Dicyandiamide and its derivatives form complexes with transition metals. Transition metal complexes have widespread use due to their biological, catalytic, and optical properties. Because of their catalytic properties, they are used as catalysts in many industrial processes such as alkene polymerization[8], olefin metathesis[9], and Wacker process[10]. Due to their biological activities, they are used as antimicrobial, antibacterial, antibiotic, antitumor drugs in the health field[11-16]. Due to their optical properties, they are used in the production of valuable optical materials such as optical modulation, optical switching, optical logic, and optical memory[17,18]. The biological, catalytic, and optical properties of transition metal complexes depend on many factors such as the type of metal, the oxidation state of the metal, the type of ligand, the number of donor atoms of the ligand and the coordination number of the complex. The change in each of these factors gives the complex a different feature and complex activity changes.

The syntheses and molecular structure determination of $[Ni(dcda\text{-}O\text{-}R)_2]^{2+}$ type four-coordinated complexes were reported by Kose et al. Also, it has been experimentally found that complexes have higher antimicrobial activity than ligands against some microorganisms[19]. However, there is no study on nonlinear optical (NLO) properties and antitumor activity of the complexes.

In this study, we aimed to determine the molecular structures of the complexes {$[Ni(dcda\text{-}O\text{-}Me)_2]^{2+}$ **(1)**, $[Ni(dcda\text{-}O\text{-}Et)_2]^{2+}$ **(2)**, $[Ni(dcda\text{-}O\text{-}^{n}Pr)_2]^{2+}$ **(3),** and $[Ni(dcda\text{-}O\text{-}^{n}Bu)_2]^{2+}$ **(4)**} by quantum chemical

calculations and to predict NLO properties and antitumor activities. For this purpose, the complexes were optimized in the gas phase at B3LYP/LANL2DZ/6-31+G(d,p) level, IR, and NMR spectra were calculated. To estimate NLO properties, some electronic structure descriptors in the gas phase were calculated and compared to reference urea. Some electronic structure identifiers were calculated in the aqueous phase to estimate the antitumor properties. In addition, molecular docking calculations were performed against the 3WZE protein. The values of the electronic structure descriptors and the data of the molecular docking studies were compared with the antitumor drug cisplatin.

Materials and Methods

Computational methods

Schematic structures of the complexes were drawn with GaussView 5.0.8[20] program. Optimization calculations were made in the gas and aqueous phase at B3LYP/LANL2DZ/6-31+G(d,p) level with Gaussian 09 AS64L-G09RevD.01 program[21]. B3LYP is a hybrid density functional theory method using Becke three-parameter exchange functional[22] and Lee-Young-Parr correlation functional[23]. LANL2DZ/6-31+G(d,p) is a mixed basis set. LANLDZ is a basis set used to represent the orbitals of the beyond third-period atoms where the inner shell electrons are modeled through an effective core potential. 6-31+G(d,p) basis set is a diffuse function and adds d functions to heavy atoms and p functions to hydrogen atoms[24]. In the aqueous phase calculations, the conductor-like polarized continuum model (C-PCM), which is the self-consistent reaction field (SCRF) method, was selected[25]. NMR chemical shifts were calculated at the same level using the Gauge-including atomic orbitals (GIAO) method[26]. TMS was taken as a reference in NMR calculations. Chemical shifts of ^{13}C-NMR and ^{1}H-NMR in the complexes were calculated from Eqn (1)[27].

$$\delta = \sum_{TMS} - \sum \quad \text{... (1)}$$

where, δ is the chemical shift, Σ_{TMS} and Σ are the shielding in carbon or hydrogen atoms in TMS and in the complex, respectively.

The complexes were optimized at B3LYP/LANL2DZ/6-31+G(d,p) level, and the urea used as reference was optimized at B3LYP/6-31+G(d,p). Ionization energy (I), electron affinity (A), energy gap (ΔE), hardness (η), softness (σ), global softness (S), electronegativity (χ), chemical potential (μ_{cp}), electrophilicity index (ω), nucleophilicity index (ε), average molecular polarizability (α), and static dipole moment (μ) values were calculated from Eqns 2 - 13[28-32].

$$I = -E_{HOMO} \quad \text{... (2)}$$

$$A = -E_{LUMO} \quad \text{... (3)}$$

$$\Delta E = E_{LUMO} - E_{HOMO} \quad \text{... (4)}$$

$$\eta = \frac{E_{LUMO} - E_{HOMO}}{2} \quad \text{... (5)}$$

$$\sigma = \frac{1}{\eta} \quad \text{... (6)}$$

$$S = \frac{1}{2\eta} \quad \text{... (7)}$$

$$\chi = -\frac{E_{HOMO} + E_{LUMO}}{2} \quad \text{... (8)}$$

$$\mu_{cp} = -\chi \quad \text{... (9)}$$

$$\omega = \frac{\mu_{cp}^2}{2\eta} \quad \text{... (10)}$$

$$\varepsilon = \frac{1}{\omega} \quad \text{... (11)}$$

$$\alpha = \frac{1}{3(\alpha_{xx} + \alpha_{yy} + \alpha_{zz})} \quad \text{... (12)}$$

$$\mu = \left(\mu_x^2 + \mu_y^2 + \mu_z^2\right)^{\frac{1}{2}} \quad \text{... (13)}$$

The complexes and cisplatin were optimized at B3LYP/LANL2DZ/6-31+G(d,p) level in the aqueous phase. Electronic structure descriptors such as I, A, ΔE, η, σ, S, χ, μ_{cp}, ω, ε, and α of the complexes and cisplatin were calculated from Eqns (2) – (12). Also, complexes and cisplatin were docked into a protein with the PDB code 3WZE. Molecular docking calculations were made with Hex 8.0.0 program[33].

Results and Discussion

Structure optimization

Molecular properties depend on the structure of the molecules. In computational chemistry, molecular structures are determined by optimization and frequency calculation. The number of imaginer frequencies is zero in the ground state molecular structures. The ground state optimized structures of the complexes were obtained in the gas phase at

B3LYP/LANL2DZ/6-31+G(d,p) level and given with the atomic labels in Fig. 1.

As can be seen from the optimized structures, the alkoxy groups bounded to the dcda ligand are located in trans positions to each other. This indicates that steric repulsions are minimal in trans structures in the gas phase and the total energies of trans structures are lower than cis structure. Also, dcda acts as a bidentate ligand and forms a five-membered chelate ring. The central nickel (II) ion environment is four coordinated. Some molecular structure parameters obtained from optimized structures are given in Table 1.

Experimental values in Table 1 are taken from reference[18], obtained in DMF solvent. Computational values were obtained in the gas phase. As seen from Table 1, the calculated lengths for complex 2 – 4 are quite compatible with experimental bond lengths. Here, the Ni31-N9 and Ni31-N24 bonds on the alkoxy group side are slightly longer than other Ni-N bonds. This can be explained by the fact that the electronegativity of the oxygen atom is higher than the nitrogen atom. Since the oxygen atom with high electronegativity has a greater inductive effect, it caused the extension of the Ni-N bond close to it.

Experimental bond angles are also quite compatible with those obtained computationally. As seen in Table 1, cis angles are calculated as 90 degrees and trans angles are calculated as 180 degrees. This result shows that the central nickel atom geometry is very

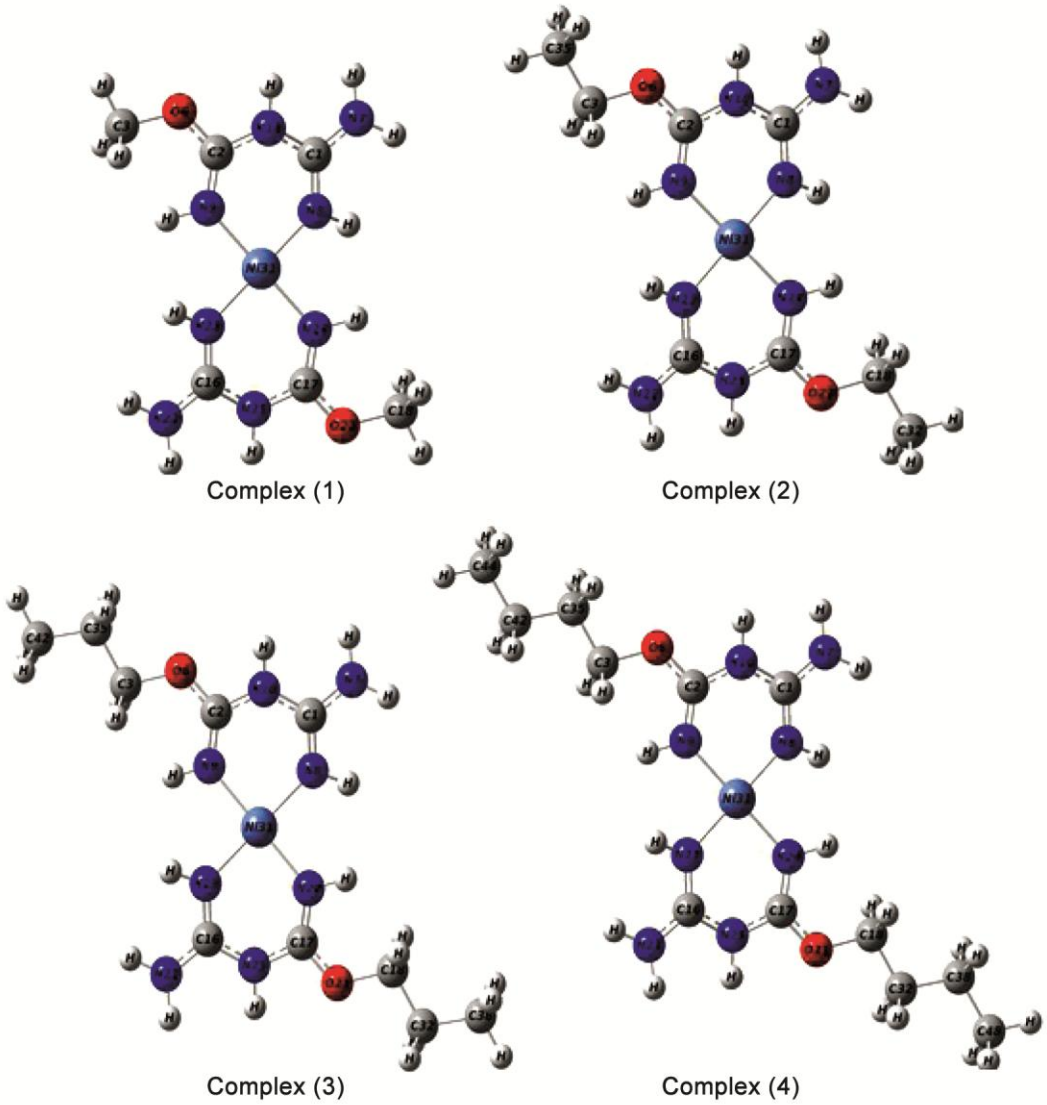

Fig. 1 — Optimized structures of the complexes obtained at B3LYP/LANL2DZ/6-31+G(d,p) level in the gas phase

Table 1 — Structural parameters of optimized complexes at B3LYP/LANL2DZ/6-31+G(d,p) level in the gas phase

	Complex (1)		Complex (2)		Complex (3)		Complex (4)	
Length (Å)	Calc.	Exp.	Calc.	Exp.	Calc	Exp.	Calc.	Exp.
Ni31-N8	1.905	-	1.904	1.863	1.905	1.864	1.905	1.862
Ni31-N9	1.910	-	1.909	1.874	1.909	1.876	1.909	1.874
Ni31-N23	1.905	-	1.904	-	1.905	-	1.905	-
Ni31-N24	1.910	-	1.909	-	1.909	-	1.909	-
				Angle (°)				
N8-Ni31-N9	89.5	-	89.5	90.3	89.5	90.3	89.5	90.3
N8-Ni31-N23	180.0	-	180.0	180.0	180.0	180.0	180.0	180.0
N8-Ni31-N24	90.5	-	90.5	89.7	90.5	89.7	90.5	89.7
N23-Ni31-N24	89.5	-	89.5	-	89.5	-	89.5	-
N9-Ni31-N23	90.5	-	90.5	-	90.5	-	90.5	-
N9-Ni31-N24	180.0	-	180.0	180.0	180.0	180.0	180.0	180.0
				Dihedral Angle (°)				
C1-N8-N23-C16	-180.0	-	-180.0	-	180.0	-	180.0	-
C2-N9-N24-C17	180.0	-	180.0	-	-180.0	-	-180.0	-
N9-N8-N24-N23	0.0	-	0.0	-	0.0	-	0.0	-
C1-C2-C16-C17	0.0	-	0.0	-	0.0	-	0.0	-

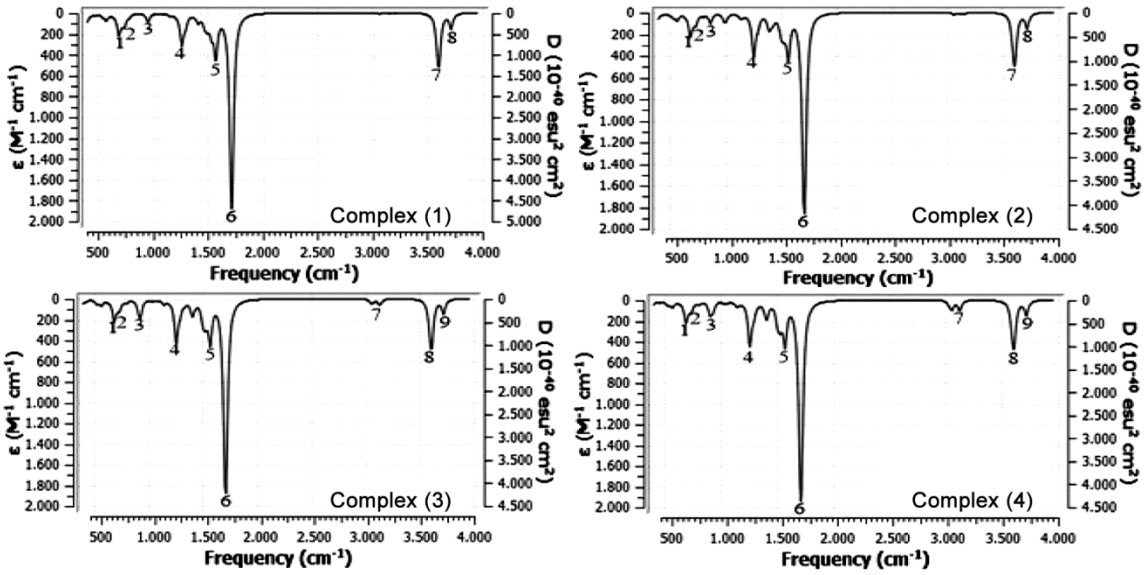

Fig. 2 — IR spectra of nickel(II) complexes containing alkoxy-derived dcda ligands

close to the square plane. The dihedral angles given in Table 1 are 180 and 0.0 degrees, indicating that the central nickel atom environment geometry is planar. Also, alteration of the alkoxy group in the dcda ligand appears to not affect the bond lengths, bond angles and dihedral angles of the complexes around the central atom.

IR Spectra and frequencies of peaks

One of the most important techniques used in determining the molecular structure is the measurement of IR spectra and labeling of the peaks. While the location of the peaks depends on the force constant of the bond and the reduced mass of the vibrating atoms, the number of peaks depends on the number of atoms in the molecule, the symmetry of the molecule, and the IR activity of the vibration. In this study, the IR spectra of complexes were calculated at B3LYP/ LANL2DZ/6-31+G(d,p) level in the gas phase and given in Fig. 2.

As seen in Fig. 2, eight peaks for complex (1) and (2) and nine peaks for complex (3) and (4) are numbered. The peaks numbered with 7 for complex (3) and (4) belong to the alkyl group C-H stretching vibrations. Although the complex (1) and (2) also have alkyl groups, their peaks are in very small

intensity. Therefore, their peaks are not taken into account. The vibrations forming the peaks given in Fig. 2 and the frequencies of the peaks are presented in Table 2. Experimental values are taken from reference[18].

The frequencies calculated in Table 2 are harmonic and the experimental frequencies are anharmonic. To obtain anharmonic frequencies from harmonic frequencies, there must be a scale factor at each calculation level. However, there is no scale factor for B3LYP/LANL2DZ/6-31+G(d,p) level in the literature. When the frequency scale factors in the literature for various levels are examined, it is seen that it varies in the range of 0.89-1.0[24]. If the harmonic frequencies in Table 2 are multiplied by a number in the range 0.89-1.0, it is seen to be quite compatible with the experimental values.

As seen in Table 2, the peaks characteristic for the complexes belong to the Ni-N, R-O, C-N, C=N, C-H, and N-H stretching vibrations. As expected, the Ni-N peak was found at low frequency and the N-H peak at the highest frequency. The fact that the force constant of the Ni-N bond is small and its reduced mass is large causes it to be observed at a lower frequency. This finding is compatible with the literature[34]. Because metal-ligand bond stretching vibrations are often observed at low frequencies. The peaks of the C-N stretching vibrations in the complexes were calculated at about 1570 cm^{-1} and the peaks of the C=N vibrations at about 1715 cm^{-1}. This finding is consistent with the bond force constant. Because the reduced masses of C-N and C=N are the same, only the bond force constants are different. Since the C=N bond force constant is greater than that of C-N, it was observed at high frequency. The frequencies of the R-O stretching vibrations fall into the single bond stretching region. R-O stretching vibrations for the complexes were observed in the range of 868-953 cm^{-1}.

NMR chemical shift values

One of the most preferred techniques in molecular structure characterization is NMR spectroscopy. By NMR spectroscopy, ^{13}C, and ^{1}H-NMR spectra of molecules can be obtained and chemical shift values can be calculated. Chemical shifts can be used to determine the equivalent atoms in molecules and to predict the molecular structure. ^{13}C-NMR and ^{1}H-NMR spectra of the complexes examined in this study were calculated in the gas phase using the GIAO method at the level of B3LYP/LANL2DZ/6-31+G(d,p). In the interpretation of NMR spectra, tetramethylsilane (TMS) was taken as a reference. TMS was optimized at B3LYP/6-31+G(d,p) level. Shielding of carbon and hydrogen atoms in TMS was obtained as 192.5 and 31.6 ppm by using GIAO method in the gas phase. Chemical shifts of ^{13}C-NMR

Table 2 — Vibrations that form high-intensity peaks and the frequencies (cm^{-1}) of the peaks calculated at B3LYP/LANL2DZ/6-31+G(d,p) level

		Complex (1)		Complex (2)	
Peak	Vibrations	Calc.	Exp.	Calc.	Exp.
1	δ_{oop}(N-H)	687.5	-	686.8	-
2	ν_{as}(Ni-N)	744.7	556	742.8	553
3	ν_{as}(R-O)	952.3	-	868.8	-
4	δ_{ip}(N-H) + ν_{s}(C-O)	1260.9	-	1256.5	-
5	ν_{as}(C-N)	1570.9	-	1571.5	-
6	ν_{as}(C=N)	1718.4	1655	1716.2	1655
7	ν_{s}(N-H+NH_2)	3605.9	3366	3609.7	3346
8	ν_{as}(NH_2)	3713.5	3455	3715.9	3446
		Complex (3)		Complex (4)	
Peak	Vibrations	Calc.	Exp.	Calc.	Exp.
1	δ_{oop}(N-H)	686.8	-	687.2	-
2	ν_{as}(Ni-N)	744.8	556	745.2	564
3	ν_{as}(R-O)	928.3	-	927.8	-
4	δ_{ip}(N-H) + ν_{s}(C-O)	1256.4	-	1256.3	-
5	ν_{as}(C-N)	1569.2	-	1569.3	-
6	ν_{as}(C=N)	1715.8	1655	1715.6	1662
7	ν(C-H)	3127.6	2977	3121.0	2941
8	ν_{s}(N-H+NH_2)	3609.2	3345	3609.4	3343
9	ν_{as}(NH_2)	3716.5	3456	3716.8	3441

ν_{as}: Asymmetric stretching, ν_{s}: Symmetric stretching, δ_{oop}: Out of plane deformation, δ_{i}: In-plane deformation, R: Alkyl group

and ^{1}H-NMR in the complexes were calculated from Eqn (1) and given in Table 3.

As seen in Table 3, carbon atoms in trans position to each other and hydrogen atoms in trans position to each other have the same chemical shift value. This finding shows that atoms in trans position to each other are equivalent. In other words, the atoms *C1* - *C16*, *C2* - *C17*, and N7*H*(1) - N22*H*(1) are equivalent. In the complexes, carbon atoms *C1, C16, C2*, and *C17* have made sp^2 hybridization and other carbon atoms have sp^3 hybridization. While the hybrid orbital s character is 0.33 in sp^2 hybridization, it is 0.25 in sp^3 hybridization. As the hybrid orbital s character increases, the atomic nuclei are less shielded by electrons. Since the less shielded nucleus has a higher chemical shift, the chemical shift value (147-153 ppm) of the carbon atoms that make sp^2 hybridization is higher than the chemical shift (15-77 ppm) of the carbon atoms that make sp^3 hybridization. In addition, since the *C2* and *C17* atoms are adjacent to the oxygen atom with higher electronegativity, it was less shielded and had a higher chemical shift value. As the carbon atoms making sp^3 hybridization move away from the electronegative oxygen atom, the chemical shift values decrease. As the carbon atoms making sp^3 hybridization move away from the electronegative oxygen atom, the chemical shift values decrease. Because the nuclei that are far from the electronegative atom are mostly shielded.

Table 3 — ^{13}C-NMR and ^{1}H-NMR chemical shift (ppm) values calculated in the gas phase for complex (1) – (4)

Labeling	Complex (1)	Complex (2)	Complex (3)	Complex (4)
C1, C16	147.5	147.5	147.5	147.5
C2, C17	154.3	153.9	154.1	154.2
C3, C18	57.1	71.5	76.5	75.8
C35, C32	-	14.7	25.5	33.7
C42, C38	-	-	9.2	21.5
C44, C48	-	-	-	15.2
N7*H(1)*,N22*H(1)*	4.7	4.7	4.7	4.6
N7*H(2)*, N22*H(2)*	4.7	4.7	4.7	4.6
N8*H*, N23*H*	2.1	2.1	2.1	2.1
N9*H*, N24*H*	3.0	2.9	2.9	2.9
N10*H*, N25*H*	6.4	6.4	6.3	6.3
C3*H(1)*, C18*H(1)*	4.8	4.2	4.0	4.0
C3*H(2)*, C18*H(2)*	3.9	4.2	3.9	3.9
C3*H(3)*, C18*H(3)*	3.9	-	-	-
C35*H(1)*, C32*H(1)*	-	1.7	2.1	2.1
C35*H(2)*, C32*H(2)*	-	1.8	2.2	2.0
C35*H(3)*, C32*H(3)*	-	1.9	-	-
C42*H(1)*, C38*H(1)*	-	-	1.8	1.3
C42*H(2)*, C38*H(2)*	-	-	0.9	1.3
C42*H(3)*, C38*H(3)*	-	-	0.8	-
C44*H(1)*, C48*H(1)*	-	-	-	1.6
C44*H(2)*, C48*H(2)*	-	-	-	1.2
C44*H(3)*, C48*H(3)*	-	-	-	1.2

For the ^{1}H-NMR chemical shift values, the hybridization type of the atom to which the proton is attached and the distance of the proton from the electronegative atom are important. As seen in Table 3, the chemical shifts of the protons (C32*H*, C35*H*, C38*H*, C42*H*, and C48*H*) bonded to carbon atoms that make sp^3 hybridization and are far from the electronegative atom range from 0.8 to 2.2 ppm, while the chemical shift values of those close to the electronegative oxygen atom (C3*H* and C18*H*) is in the range of 3.9-4.8 ppm. N10 and N25 atoms have both high s-character and high electronegativity. Therefore, the chemical shift value (6.4 ppm) of the hydrogen-bonded to N10*H* and N25*H* atoms was found to be the highest. The chemical shift value (2.1 ppm) of N8*H* and N23*H* protons is lower than N9*H*, N24*H* protons (2.9 - 3.0 ppm). This is because the N9*H*, N24*H* protons are neighbor to the electronegative oxygen atom.

According to the information given so far, the gas-phase structures of the studied complexes were verified by optimization at B3LYP/LANL2DZ/6-31+G(d,p) level, peak frequencies calculated in IR and chemical shift values obtained from NMR spectra.

NLO properties of the complexes

Materials with nonlinear optical properties are still an active field of study because they are used in areas such as modern communication technology, data storage and optical signal processing[32]. Therefore, it is important to synthesize materials with NLO properties and to investigate whether the synthesized substances have NLO properties. In computational chemistry, NLO properties are estimated by various electronic structure descriptors. As seen from Eqn (2)-(11), frontier orbital energies are used to calculate many electronic structure descriptors. Frontier orbital contour diagrams and energies are given in Fig. 3.

As can be seen from Fig. 3, HOMO generally consists of the linear combination of the orbitals of the N7, C1, N8, Ni31, N23, C16, and N22 atoms, or the electrons in HOMO are located on these atoms. Whereas, LUMO is delocalized on C1, C2, N8, N9 Ni31, N23, N24, C16, C17 atoms. Both

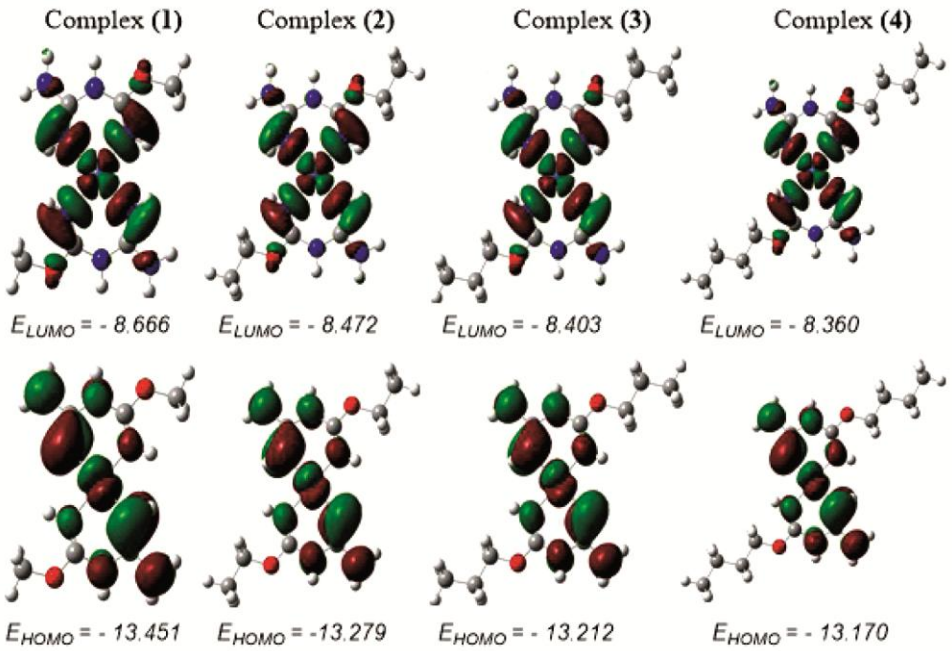

Fig. 3 — HOMO and LUMO contour diagrams and energies of the studied complexes

Table 4 — Calculated electronic structure descriptors for complex (1) – (4) and urea in the gas phase

Descriptor	Complex (1)	Complex (2)	Complex (3)	Complex (4)	Urea
E_{LUMO}[1]	-8.666	-8.472	-8.403	-8.360	-0.373
E_{HOMO}[1]	-13.451	-13.279	-13.212	-13.170	-7.318
I[1]	13.451	13.279	13.212	13.170	7.318
A[1]	8.666	8.472	8.403	8.360	0.373
ΔE[1]	4.785	4.806	4.809	4.810	6.944
η[1]	2.392	2.403	2.404	2.405	3.472
σ[2]	0.418	0.416	0.416	0.416	0.288
S[2]	0.209	0.208	0.208	0.208	0.144
χ[1]	11.059	10.876	10.807	10.765	3.846
μ_{cp}[1]	-11.059	-10.876	-10.807	-10.765	-3.846
ω[1]	25.558	24.608	24.288	24.091	2.130
ε[2]	0.039	0.041	0.041	0.042	0.470
α[3]	159.389	186.135	211.273	237.264	32.735
μ[4]	$2.2x10^{-4}$	$2.2x10^{-4}$	$11.2x10^{-4}$	$3.0x10^{-4}$	4.566

[1]eV, [2]eV^{-1}, [3]a.u, [4]Debye,

HOMO and LUMO energies increase from the complex (1) to complex (4). Some electronic structure descriptors such as ionization energy (I), electron affinity (A), energy gap (ΔE), hardness (η), softness (σ), global softness (S), absolute electronegativity (χ), chemical potential (μ_{cp}), electrophilicity index (ω), nucleophilicity index (ε), average molecular polarizability (α), and static dipole moment (μ) were calculated in the gas phase using frontier molecular orbital energies for the complexes and reference urea and given in Table 4.

Ionization energy and electron affinity values are equal to the opposite sign of HOMO and LUMO energies according to the Koopmans theorem[35]. The ionization energy of molecules shows the tendency to give electrons, and the electron affinity indicates the tendency to receive. In molecules with high ionization energy and electron affinity, electrons are more attracted by nuclei and electron mobility and NLO feature decrease.

A smaller energy gap indicates that charge transfer within the molecule is easier and the NLO property is

high. Also, molecules with low hardness, high softness and global softness have high NLO properties. Absolute electronegativity is the arithmetic mean of ionization energy and electron affinity values. As the absolute electronegativity value decreases, the electrons move more easily, the charge transfer within the molecule becomes easier and the NLO activity increases.

The chemical potential is the partial molar Gibbs free energy and indicates the ability of the molecule to work. The lower the chemical potential, the higher is the NLO activity. According to Parr et al., the electrophilicity index is a measure of energy reduction due to the flow of electrons between the acceptor and the donor[36]. According to this definition, more electron flow and more energy reduction are expected in the donor-acceptor interaction of a molecule with a high electrophilicity index. Therefore, as the electrophilicity index increases, the NLO feature increases. Since the nucleophilicity index is defined as the inverse of the electrophilicity index, NLO activity increases as the nucleophilicity index decreases.

The average molecular polarizability gives the softness of the electron cloud of the molecule. Increasing the softness of the electron cloud causes the NLO feature to increase. A static dipole moment is a quantitative measure of the asymmetry of the charge distribution in the molecule. As the asymmetry in charge distribution increases, electrons move more easily and the NLO feature increases. Considering these evaluations, the NLO activity ranking of the complexes and urea were made and given in Table 5.

Table 5 — NLO activity ranking for complex (1) – (4) and urea according to **c**alculated electronic structure descriptors

Descriptor	NLO activity ranking
I, A	Urea > Complex (4) Complex (3) > Complex (2) > Complex (1)
ΔE, η, σ, S	Complex (1) > Complex (2) > Complex (3) > Complex (4) > Urea.
χ	Urea > Complex (4) > Complex (3) > Complex (2) > Complex (1)
μ_{cp}	Complex (1) > Complex (2) > Complex (3) > Complex (4) > Urea.
ω, ε	Complex (1) > Complex (2) > Complex (3) > Complex (4) > Urea.
α	Complex (4) > Complex (3) > Complex (2) > Complex (1) > Urea.
μ	Urea > Complex (3) > Complex (4) > Complex (1) = Complex (2)

Considering the rankings in Table 5, it is seen that the complexes have higher NLO properties than urea, except for I, A, χ, and μ ranking. All of the complexes can be used to produce NLO material. Also, complex (1) can be considered as a better NLO material than others. Because complex (1) is more active than other complexes compared to most of the calculated electronic structure descriptors. Although the dipole moment of the complexes is quite close to zero, NLO activities are higher than the reference urea because of the π-electron delocalization and the complex structures being planar. NLO properties increase because of the π-electron delocalization and planarity of the structure.

Antitumor activity

In computational chemistry, anti-tumor activities of complexes can be estimated by calculating electronic structure descriptors or by docking complexes against certain proteins. If the findings obtained from the electronic structure descriptors and the findings from the molecular docking calculations are compatible, the estimation becomes stronger. Since most of the biological events occur in the aqueous environment, these processes should be carried out in the aqueous phase.

Electronic structure descriptors

The complexes and the cisplatin used as reference were optimized at the B3LYP/LANL2DZ/6-31+G(d,p) level in the aqueous phase using the C-PCM model to predict anti-tumor activities. Some electronic structure descriptors for optimized structures were calculated in the aqueous phase from Eqn (2) – (12) and given in Table 6.

When discussing antitumor activity, the properties of both the complex and the target protein should be considered. Some electronic properties of the complexes are given in Table 6. Proteins can be considered as macromolecules. In general, ionization energy (I), electron affinity (A), energy gap (ΔE), hardness (η), absolute electronegativity (χ), electrophilicity index (ω) are low for macromolecules, whereas softness (σ), global softness (S), chemical potential (μ_{cp}), nucleophilicity index (ε), and average molecular polarizability (α) are high. Soft-soft or large-large interactions are known to be stronger interactions than soft-hard or large-small interactions. Accordingly, complex (1) – (4) and cisplatin antitumor activity ranking against a macromolecule are given in Table 7.

Table 6 — Some electronic structure descriptors for complex (1)-(4) and cisplatin calculated at B3LYP/LANL2DZ/6-31+G(d,p) level in the aqueous phase

Descriptor	Complex (1)	Complex (2)	Complex (3)	Complex (4)	Cisplatin
E_{LUMO}[1]	-2.479	-2.465	-2.454	-2.464	-1.932
E_{HOMO}[1]	-7.251	-7.218	-7.238	-7.197	-6.604
I[1]	7.251	7.218	7.238	7.197	6.604
A[1]	2.479	2.465	2.454	2.464	1.932
ΔE[1]	4.772	4.753	4.784	4.733	4.672
η[1]	2.386	2.376	2.392	2.366	2.336
σ[2]	0.419	0.421	0.418	0.423	0.428
S[2]	0.209	0.210	0.209	0.211	0.214
χ[1]	4.865	4.841	4.846	4.830	4.268
μ_{cp}[1]	-4.865	-4.841	-4.846	-4.830	-4.268
ω[1]	4.960	4.931	4.909	4.929	3.899
ε[2]	0.202	0.203	0.204	0.203	0.256
α[3]	205.1	236.5	267.8	297.8	116.9

[1]eV, [2]eV^{-1}, [3]a.u.

Table 7 — Antitumor activity ranking for complex (1) - (4) and cisplatin according to **c**alculated electronic structure descriptors

Descriptor	Antitumor activity ranking
I, χ, μ_{cp}	cisplatin > Complex (4) > Complex (2) > Complex (3) > Complex (1)
A, ω, ε	cisplatin > Complex (3) > Complex (4) > Complex (2) > Complex (1)
ΔE, η, σ	cisplatin > Complex (4) > Complex (2) > Complex (1) > Complex (3)
S	cisplatin > Complex (4) > Complex (2) > Complex (1) = Complex (3)
α	Complex (4) > Complex (3) > Complex (2) > Complex (1) > cis-platin

Except for the average molecular polarizability order, the rankings in Table 7 show that the antitumor activity of the complexes is lower than cisplatin. These results do not mean that the complexes have no antitumor activity. According to the quantitative structure-activity relationship (QSAR) model, electronic structure descriptors do not contribute equally to antitumor activity[37]. That is, the antitumor activity can only result from average molecular polarizability.

Molecular docking studies

Molecular docking is the process of finding the best match and interaction between two molecules. The best interaction is represented by binding energy. Binding energy includes interactions such as van der Waals interactions, electrostatic interactions, hydrogen bonds, hydrophobic interactions. The magnitude of the binding energy is a measure of the stability of the ligand-receptor complex.

Previous studies show that inhibition of vascular endothelial growth factor receptor-2 (VEGFR-2) is one of the anticancer mechanisms[38]. Therefore, VEGFR-2 was chosen as the target protein in this study. The protein data bank (PDB) code of VEGFR-2 is 3WZE. Molecular docking calculations were made between complex (**1**) – (**4**) and 3WZE cell lines. Hex 8.0.0 docking program was used in calculations. Docking poses of the complex (**1**) – (**4**) against 3WZE cell lines are given in Fig. 4.

As seen in Fig. 4, complexes almost interacted with the same region in the 3WZE protein. This zone, where complexes enter, is the active zone of 3WZE cells. Binding energy is maximum in this region. Binding energies for complex (**1**), complex (**2**), complex (**3**), and complex (**4**) were calculated as -262.1, -295.9, -329.7, and -309.0 kcal/mol, respectively. Reference cisplatin was also docked against the same cell line under the same conditions. The binding energy between cisplatin and 3WZE cell lines was calculated as -258.4 kcal/mol. These results show that the binding energy between the complex **(1)** – **(4)** and 3WZE cell lines is greater than that of the cisplatin. Therefore, complex **(1)-(4)** can be considered as an anticancer drug candidate. The anticancer activity ranking of the complexes examined according to the binding energies against the 3WZE cell lines is as follows:

Cisplatin< Complex (**1**)< Complex (**2**)< Complex (**4**)< Complex (**3**).

According to these findings, it can be said that complex (**3**) is the most suitable drug candidate for VEGFR-2.

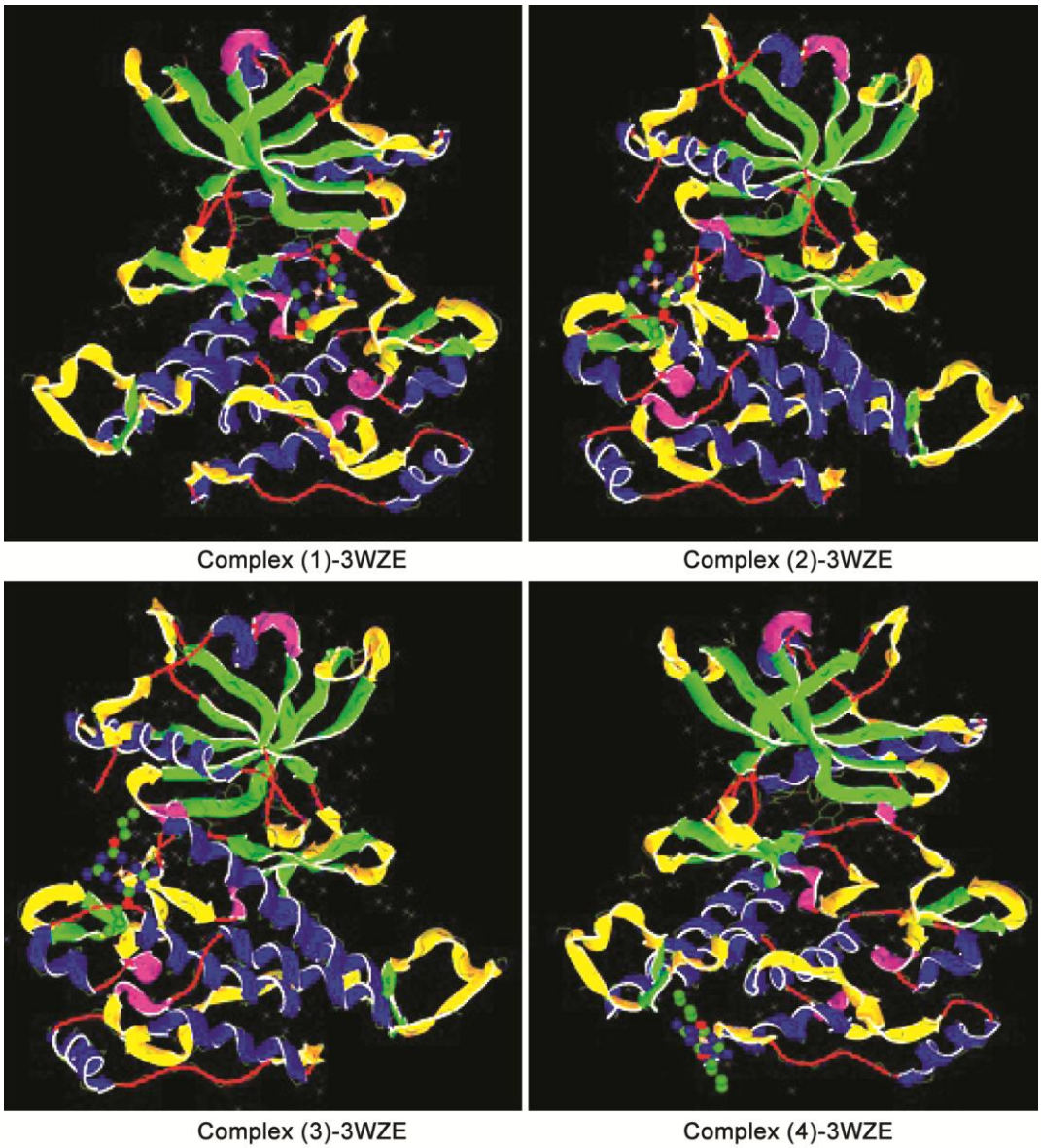

Fig. 4 — Docking poses of complex (1) – (4) against 3WZE cell lines

Conclusions

$[Ni(dcda\text{-}O\text{-}Me)_2]^{2+}$ **(1)**, $[Ni(dcda\text{-}O\text{-}Et)_2]^{2+}$ **(2)**, $[Ni(dcda\text{-}O\text{-}^{n}Pr)_2]^{2+}$ **(3)**, and $[Ni(dcda\text{-}O\text{-}^{n}Bu)_2]^{2+}$ **(4)** complexes were optimized in the gas phase at B3LYP/LANL2DZ/6-31+G(d,p) level. Molecular structure parameters, IR, and NMR spectra of the complexes were calculated. Molecular structure parameters, IR, and NMR spectra showed that the central atom environment geometry in the complexes is a distorted square plane and the alkoxy groups in the ligands are located in a trans position. It was estimated that complex (**1**) is the most suitable compound to produce optical material according to electronic structure descriptors calculated in the gas phase. According to the electronic structure descriptors, the antitumor activity of the complexes was estimated to be lower than cisplatin. Molecular docking studies against the 3WZE cell lines showed that the antitumor activity of all complexes was higher than cisplatin and complex (**3**) had the highest antitumor activity.

Acknowledgement

The authors are grateful for their support to the Sivas Cumhuriyet University, Scientific Research Unit (Project No: F-578).

References

1 Jalovy Z, Padelkova Z, Jirasko R, Matyas R, Holcapek M, Nemec O & Miskova L, *Polyhedron*, 44 (2012) 88.

2 Baker W A & Daniels M, *J Inorg Nuclear Chem*, 25 (1963) 1194.

3 Panda P K, Mishra S B & Mohapatra B K, *J Inorg Nucr Chem*, 42 (1980) 497.

4 Ray R K, Bandyopadhyay M K & Kauffman G B, *Polyhedron*, 8 (1989) 757.

5 Singh O I, Damayanti M, Singh N R, Singh R H, Mohapatra M & Kadam R M, *Polyhedron*, 24 (2005) 909.

6 Devi S P, Devi R B, Devi N S, Singh L J & Singh R H, *Polyhedron*, 47 (2012) 1.

7 Williams P A, Ferrer E G, Baeza N, Piro O E, Castellano E E & Baran E J, *Z Anorg Allg Chem*, 631 (2005) 1502.

8 Kissin Y V & Goldman A S, *Macromol Chem Phys*, 210 (2009) 1942.

9 Hughes D, Wheeler P & Ene D, *Org Process Res Dev*, 21 (2017) 1938.

10 Keith J A & Henry P M, *Angew Chem Int Ed*, 48 (2009) 9038.

11 Warra A A, *J chem Pharm Res*, 3 (2011) 951.

12 Selvaganapathy M & Raman N, *J Chem Biol Ther*, 1 (2016) 2572.

13 Shokohi-Pour Z, Chiniforoshan H, Sabzalian M R, Esmaeili S A & Momtazi-borojeni A A, *J Biomol Struct Dyn*, 36 (2018) 532.

14 Chohan Z H, Sumrra S H, Youssoufi M H & Hadda T B, *Eur J Med Chem*, 45 (2010) 2739.

15 Bergamo A, Dyson P J & Sava G, *Coord Chem Rev*, 360 (2018) 17.

16 Dilruba S & Kalayda G V, *Cancer Chemother Pharmacol*, 77 (2016) 1103.

17 Xue X, Wang H, Han Y & Hou H, *Dalton Trans*, 47 (2018) 13.

18 Prasad G K, Prashanth S S P, Srivastava S, Rao G N & Babu D R, *Open Chem*, 15 (2017) 283.

19 Kose M, Duman S E, McKee V, Akyol I & Kurtoglu M, *Inorg Chim Acta*, 462 (2017) 281.

20 Dennington R D, Keith T A & Millam C M, *Gauss View 5.0 Wallingford. In CT* (2009).

21 Frisch M J, Trucks G W, Schlegel H B, Scuseria G E, Robb M A, Cheeseman J R & Nakatsuji H, *Gaussian09 Revision D. 01, Gaussian Inc. Wallingford CT* (2009). See also: URL: http://www. gaussian. com.

22 Becke A D, *Phy Rev A*, 38 (1988) 3098.

23 Lee C, Yang W & Parr R G, *Phy Rev B*, 37 (1988) 785.

24 Foresman J B & Frisch A, *Exploring chemistry with electronic structure methods: a guide to using Gaussian* (1996).

25 Cossi M, Rega N, Scalmani G & Barone V, *J Comput Chem*, 24 (2003) 669.

26 Wolff S K & Ziegler T, *J Chem Phy*, 109 (1998) 895.

27 Güveli Ş, Özdemir N, Bal-Demirci T, Ülküseven B, Dinçer M & Andaç Ö, *Polyhedron*, 29 (2010) 2393.

28 Kose M, Ceyhan G & Karakaş D, *J Coord Chem*, 69 (2016), 497.

29 Rawat P & Singh R N, *J Mol Struct*, 1084 (2015) 326.

30 Odabaşoğlu M, Albayrak Ç, Koşar B & Büyükgüngör O, *Spectrochim Acta Part A: Mol Biomol Spectrosc*, 92 (2012) 357.

31 Erkan S & Karakaş D, *J Mol Struct*, 1199 (2020) 127054.

32 Abdel-Rahman L H, Abu-Dief A M, Moustafa H & Abdel-Mawgoud A A H, *Arab J Chem*, 13 (2020) 649.

33 Ritchie D & Orpailleur T, *Hex 8.0. 0 User Manual*, (1996).

34 Devi N S, Singh L J, Devi S P, Singh R B, Singh R H, Rajeswari B & Kadam R M, *J Coord Chem*, 64 (2011) 4108.

35 Manne R & Åberg T, *Chem Phy Letters*, 7 (1970) 282.

36 Parr R G, Szentpaly L V & Liu S, *J Am Chem Soc*, 121 (1999) 1922.

37 Galimberti F, Moretto A & Papa E, *Water Res*, 174 (2020) 115583.

38 Sayin K, Kariper S E, Taştan M, Sayin T A & Karakaş D, *J Mol Struct*, 1176 (2019) 478.